

# FIRST RESULTS FROM THE SUDBURY NEUTRINO OBSERVATORY

G.A. McGREGOR<sup>a</sup>

*Department of Physics, Denys Wilkinson Building, Keble Road, Oxford OX1 3RH, U.K.*

The Sudbury Neutrino Observatory (SNO) is a water imaging Čerenkov detector. Utilising a 1 kilotonne ultra-pure D<sub>2</sub>O target, it is the first experiment to have equal sensitivity to all flavours of active neutrinos. This allows a solar-model independent test of the neutrino oscillation hypothesis to be made. Solar neutrinos from the decay of <sup>8</sup>B have been detected at SNO by the charged-current (CC) interaction on the deuteron and by the elastic scattering (ES) of electrons. While the CC interaction is sensitive exclusively to  $\nu_e$ , the ES interaction has a small sensitivity to  $\nu_\mu$  and  $\nu_\tau$ . In this paper, the recent solar neutrino results from the SNO experiment are presented. The measured ES interaction rate is found to be consistent with the high precision ES measurement from the Super-Kamiokande experiment. The  $\nu_e$  flux deduced from the CC interaction rate in SNO differs from the Super-Kamiokande ES measurement by  $3.3\sigma$ . This is evidence of an active neutrino component, in addition to  $\nu_e$ , in the solar neutrino flux. These results also allow the first experimental determination of the active <sup>8</sup>B neutrino flux from the Sun, and this is found to be in good agreement with solar model predictions.

## 1 Introduction

Over the past 30 years, solar neutrino experiments<sup>1,2,3,4,5,6</sup> have measured fewer neutrinos than are predicted by models of the Sun.<sup>7,8</sup> A comparison of the predicted and observed solar neutrino fluxes for these experiments are shown in table 1. These observations can be explained if the solar models are incomplete or neutrinos undergo a flavour changing process while in transit to

---

<sup>a</sup>for the SNO Collaboration: Q.R. Ahmad, R.C. Allen, T.C. Andersen, J.D. Anglin, G. Bühler, J.C. Barton, E.W. Beier, M. Bercovitch, J. Bigu, S. Biller, R.A. Black, I. Blevis, R.J. Boardman, J. Boger, E. Bonvin, M.G. Boulay, M.G. Bowler, T.J. Bowles, S.J. Brice, M.C. Browne, T.V. Bullard, T.H. Burritt, K. Cameron, J. Cameron, Y.D. Chan, M. Chen, H.H. Chen, X. Chen, M.C. Chon, B.T. Cleveland, E.T.H. Clifford, J.H.M. Cowan, D.F. Cowen, G.A. Cox, Y. Dai, X. Dai, F. Dalnoki-Veress, W.F. Davidson, P.J. Doe, G. Doucas, M.R. Dragowsky, C.A. Duba, F.A. Duncan, J. Dunmore, E.D. Earle, S.R. Elliott, H.C. Evans, G.T. Ewan, J. Farine, H. Fergani, A.P. Ferraris, R.J. Ford, M.M. Fowler, K. Frame, E.D. Frank, W. Frati, J.V. Germani, S. Gil, A. Goldschmidt, D.R. Grant, R.L. Hahn, A.L. Hallin, E.D. Hallman, A. Hamer, A.A. Hamian, R.U. Haq, C.K. Hargrove, P.J. Harvey, R. Hazama, R. Heaton, K.M. Heeger, W.J. Heintzelman, J. Heise, R.L. Helmer, J.D. Hepburn, H. Heron, J. Hewett, A. Hime, M. Howe, J.G. Hykawy, M.C.P. Isaac, P. Jagam, N.A. Jelly, C. Jillings, G. Jonkmans, J. Karn, P.T. Keener, K. Kirch, J.R. Klein, A.B. Knox, R.J. Komar, R. Kouzes, T. Kutter, C.C.M. Kyba, J. Law, I.T. Lawson, M. Lay, H.W. Lee, K.T. Lesko, J.R. Leslie, I. Levine, W. Locke, M.M. Lowry, S. Luoma, J. Lyon, S. Majerus, H.B. Mak, A.D. Marino, N. McCauley, A.B. McDonald, D.S. McDonald, K. McFarlane, G. McGregor, W. McLatchie, R. Meijer Drees, H. Mes, C. Miiffin, G.G. Miller, G. Milton, B.A. Moffat, M. Moorhead, C.W. Nally, M.S. Neubauer, F.M. Newcomer, H.S. Ng, A.J. Noble, E.B. Norman, V.M. Novikov, M. O'Neill, C.E. Okada, R.W. Ollerhead, M. Omori, J.L. Orrell, S.M. Oser, A.W.P. Poon, T.J. Radcliffe, A. Roberge, B.C. Robertson, R.G.H. Robertson, J.K. Rowley, V.L. Rusu, E. Saettler, K.K. Schaffer, A. Schuelke, M.H. Schwendener, H. Seifert, M. Shatkay, J.J. Simpson, D. Sinclair, P. Skensved, A.R. Smith, M.W.E. Smith, N. Starinsky, T.D. Steiger, R.G. Stokstad, R.S. Storey, B. Sur, R. Tafirout, N. Tagg, N.W. Tanner, R.K. Taplin, M. Thorman, P. Thornewell P.T. Trent, Y.I. Tserkovnyak, R. Van Berg, R.G. Van de Water, C.J. Virtue, C.E. Waltham, J.-X. Wang, D.L. Wark, N. West, J.B. Wilhelmy, J.F. Wilkerson, J. Wilson, P. Wittich, J.M. Wouters, M. Yeh.

Table 1: Summary of solar neutrino observations at different solar neutrino detectors.

Experiment	Measured Flux	SSM Flux <sup>7</sup>
Homestake <sup>1</sup>	$2.56 \pm 0.16(stat.) \pm 0.16(sys.)$ SNU	$7.6^{+1.3}_{-1.1}$ SNU
SAGE <sup>2</sup>	$67.2^{+7.2}_{-7.0}(stat.)^{+3.5}_{-3.0}(sys.)$ SNU	$128^{+9}_{-7}$ SNU
Galex <sup>3</sup>	$77.5 \pm 6.2(stat.)^{+4.3}_{-4.7}(sys.)$ SNU	$128^{+9}_{-7}$ SNU
GNO <sup>4</sup>	$65.8^{+10.2}_{-9.6}(stat.)^{+3.4}_{-3.6}(sys.)$ SNU	$128^{+9}_{-7}$ SNU
Kamiokande <sup>5</sup>	$2.80 \pm 0.19(stat.) \pm 0.33(sys.) \times 10^6 \text{ cm}^{-2} \text{ s}^{-1}$	$5.05(1^{+0.20}_{-0.16}) \times 10^6 \text{ cm}^{-2} \text{ s}^{-1}$
Super-Kamiokande <sup>6</sup>	$2.32 \pm 0.03(stat.)^{+0.08}_{-0.07}(sys.) \times 10^6 \text{ cm}^{-2} \text{ s}^{-1}$	$5.05(1^{+0.20}_{-0.16}) \times 10^6 \text{ cm}^{-2} \text{ s}^{-1}$

the Earth, the most accepted of which is neutrino oscillations. This puzzle is known as the solar neutrino problem.

## 2 The Sudbury Neutrino Observatory

### 2.1 The SNO Detector

SNO<sup>9</sup> is an imaging water Čerenkov detector located at a depth of 2092 m (6010 m of water equivalent) in the INCO, Ltd. Creighton mine near Sudbury, Ontario. The detector, shown in figure 1, is situated in a large barrel shaped cavity 22 m in diameter and 34 m in height. The 1 kilotonne ultra-pure D<sub>2</sub>O target is contained within a transparent acrylic vessel (AV) 12 m in diameter and 5.5 cm thick. A 17.8 m diameter geodesic sphere (PSUP - photomultiplier support structure) surrounds the AV and supports 9456 inward looking and 91 outward looking 20 cm photomultiplier tubes (PMTs). The PSUP is supported by steel ropes attached to the deck. The remaining volume is filled with ultra-pure H<sub>2</sub>O which acts as a cosmic ray veto and as a shield from naturally occurring radioactivity in both the construction materials and the surrounding rock. The light water also supports the D<sub>2</sub>O and AV with the remaining weight supported by 10 Vectran rope loops.

A physics event trigger is generated in the detector when 18 or more PMTs exceed a threshold of  $\sim 0.25$  photo-electrons within a coincidence time window of 93 ns. The trigger reaches 100% efficiency when the PMT multiplicity is  $\geq 23$ . The instantaneous trigger rate is about 15-20 Hz, of which 6-8 Hz are physics triggers and the rest are diagnostic triggers.

### 2.2 Neutrino Interactions in SNO

By utilising a D<sub>2</sub>O target, the SNO detector is capable of simultaneously measuring the flux of electron type neutrinos and the total flux of all active neutrinos from <sup>8</sup>B decay in the Sun through the following interactions:

$$\begin{aligned}
 \nu_e + d &\rightarrow p + p + e^- && (CC) \\
 \nu_x + d &\rightarrow \nu_x + p + n && (NC) \\
 \nu_x + e^- &\rightarrow \nu_x + e^- && (ES)
 \end{aligned}$$

The charged-current (CC) interaction on the deuteron is sensitive exclusively to  $\nu_e$ , and the neutral-current (NC) interaction has equal sensitivity to all active neutrino flavours ( $\nu_x, x=e,\mu,\tau$ ). Elastic scattering (ES) on the electron is also sensitive to all active flavours, but has enhanced sensitivity to  $\nu_e$ .

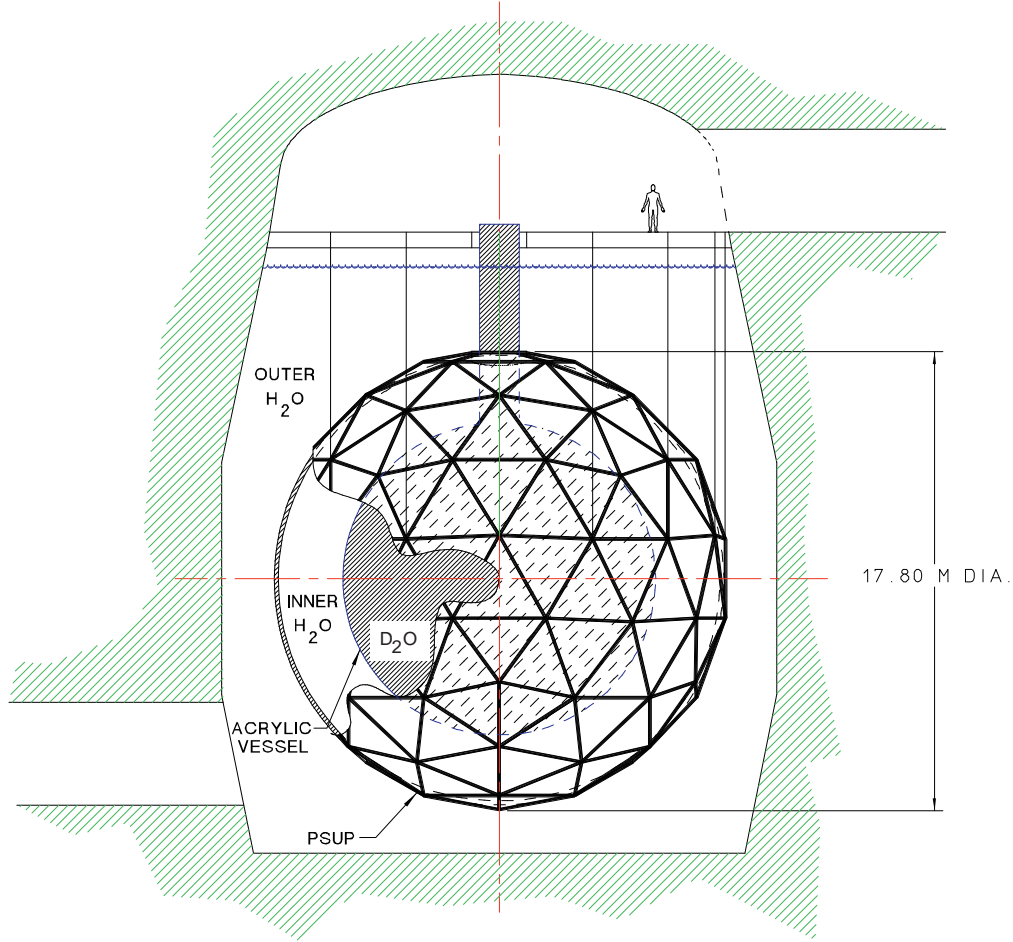


Figure 1: A cross-sectional view of the SNO detector.

### 3 Results from SNO

The results presented here are the recent results from the SNO collaboration.<sup>10</sup> Full details of the analysis will not be presented here; readers are encouraged to consult the original paper. The results are from data recorded between Nov. 2, 1999 and Jan. 15, 2001, corresponding to 240.95 days of live time. The neutrino fluxes deduced from the CC and ES interactions at SNO are:

$$\begin{aligned}\Phi_{\text{SNO}}^{\text{CC}} &= 1.75 \pm 0.07(\text{stat.})_{-0.11}^{+0.12}(\text{sys.}) \pm 0.05(\text{theor.}) \times 10^6 \text{ cm}^{-2} \text{ s}^{-1} \\ \Phi_{\text{SNO}}^{\text{ES}} &= 2.39 \pm 0.34(\text{stat.})_{-0.14}^{+0.16}(\text{sys.}) \times 10^6 \text{ cm}^{-2} \text{ s}^{-1}\end{aligned}$$

where the theoretical uncertainty is the CC cross section uncertainty.<sup>11</sup> The difference between  $\Phi_{\text{SNO}}^{\text{CC}}$  and  $\Phi_{\text{SNO}}^{\text{ES}}$  is  $0.64 \pm 0.40 \times 10^6 \text{ cm}^{-2} \text{ s}^{-1}$ , or  $1.6\sigma$ . The ratio of  $\Phi_{\text{SNO}}^{\text{CC}}$  to the predicted  ${}^8\text{B}$  solar neutrino flux given by the BPB01 solar model<sup>7</sup> is  $0.347 \pm 0.029$  where all the uncertainties are added in quadrature.

The Super-Kamiokande<sup>6</sup> experiment has made a high precision measurement of the  ${}^8\text{B}$  solar neutrino flux deduced from the ES interaction:

$$\Phi_{\text{SK}}^{\text{ES}} = 2.32 \pm 0.03(\text{stat.})_{-0.07}^{+0.08}(\text{sys.}) \times 10^6 \text{ cm}^{-2} \text{ s}^{-1}$$

The measurements  $\Phi_{\text{SNO}}^{\text{ES}}$  and  $\Phi_{\text{SK}}^{\text{ES}}$  are consistent. Assuming that the systematic errors are

Table 2: Systematic uncertainties on fluxes.

Error source	CC error (percent)	ES error (per cent)
Energy scale	-5.2, +6.1	-3.5, +5.4
Energy resolution	$\pm 0.5$	$\pm 0.3$
Energy scale non-linearity	$\pm 0.5$	$\pm 0.4$
Vertex accuracy	$\pm 3.1$	$\pm 3.3$
Vertex resolution	$\pm 0.7$	$\pm 0.4$
Angular resolution	$\pm 0.5$	$\pm 2.2$
High energy $\gamma$ 's	-0.8, +0.0	-1.9, +0.0
Low energy background	-0.2, +0.0	-0.2, +0.0
Instrumental background	-0.2, +0.0	-0.6, +0.0
Trigger efficiency	0.0	0.0
Live time	$\pm 0.1$	$\pm 0.1$
Cut acceptance	-0.6, +0.7	-0.6, +0.7
Earth orbit eccentricity	$\pm 0.1$	$\pm 0.1$
$^{17}\text{O}$ , $^{18}\text{O}$	0.0	0.0
Experimental uncertainty	-6.2, +7.0	-5.7, +6.8
Cross section	3.0	0.5
Solar Model	-16, +20	-16, +20

normally distributed, the difference between  $\Phi_{\text{SNO}}^{\text{CC}}$  and  $\Phi_{\text{SK}}^{\text{ES}}$  is  $0.57 \pm 0.17 \times 10^6 \text{ cm}^{-2} \text{ s}^{-1}$ , or  $3.3\sigma$ . The probability that  $\Phi_{\text{SNO}}^{\text{CC}}$  is a  $\geq 3.3\sigma$  downward fluctuation is 0.04%.

The CC energy spectrum was also extracted from the data and no evidence for spectral distortions was found.

### 3.1 Systematic Uncertainties

The systematic uncertainties in the SNO results are shown in table 2. The dominant uncertainties are the energy scale and the reconstruction accuracy. The reconstruction accuracy was determined using a triggered  $^{16}\text{N}$  6.13 MeV  $\gamma$ -ray source.<sup>12</sup> Figure 2 shows some of the results of such a study. When the source was operated at low rate, the reconstruction accuracy was observed to become worse. This was found to be because the PMT calibration characteristics were dependent on the readout history of the PMT, compounded in non-central  $^{16}\text{N}$  calibration runs by a readout rate gradient across the detector. This was addressed by the HCA calibration<sup>13</sup> which allowed the reconstruction accuracy of neutrino events to be correctly estimated at  $\sim 3\%$  (rather than  $\sim 10\%$ ).

### 3.2 Total Active $^8\text{B}$ Neutrino Flux

Remembering that SNO's CC measurement is only sensitive to electron neutrinos, whereas Super-Kamiokande's ES measurement has a weak sensitivity to all active flavours, one can deduce the total  $^8\text{B}$  solar neutrino flux. Stated explicitly, the experimental sensitivities to neutrino flavours are:

$$\Phi_{\text{SNO}}^{\text{CC}} = \Phi_e ; \quad \Phi_{\text{SK}}^{\text{ES}} = \epsilon \Phi_{\mu\tau}$$

where  $\Phi_{\mu\tau}$  is the combined  $\nu_\mu$  and  $\nu_\tau$  flux and  $\epsilon=1/6.481$ . These equations can be solved for  $\Phi_e$  and  $\Phi_{\mu\tau}$ . This is shown graphically in figure 3.

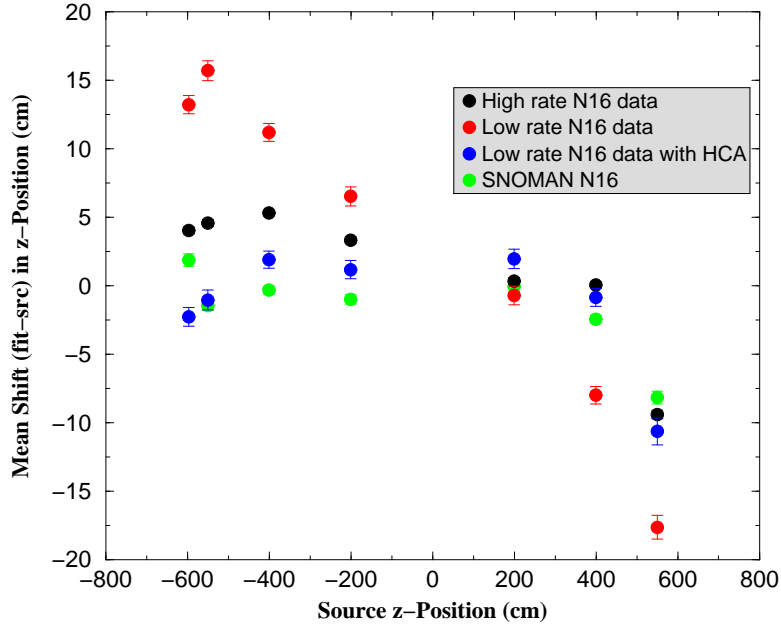


Figure 2: The shift in the reconstructed position of the  $^{16}\text{N}$  source as a function of source position. The HCA calibration corrects the inward shift seen in the low rate  $^{16}\text{N}$  data. SNOMAN is the SNO Monte Carlo package.

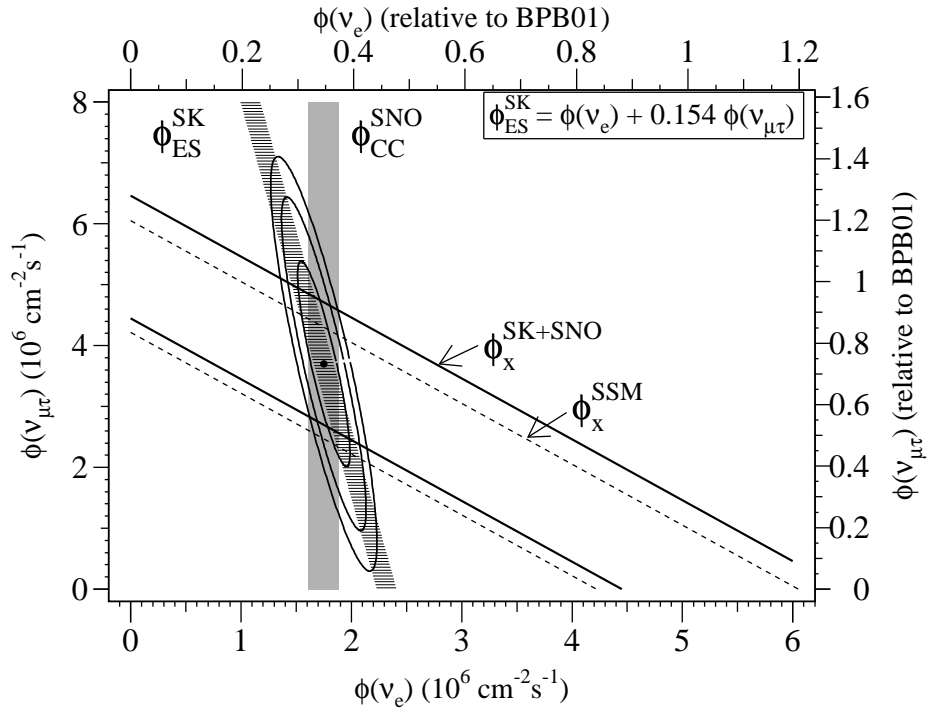


Figure 3: The flux of  $^8\text{B}$  solar neutrinos which are  $\mu$  or  $\tau$  flavour vs. the flux of electron neutrinos as deduced from the SNO and Super-Kamiokande results. The diagonal bands show the total  $^8\text{B}$  flux as predicted by the BPB01 (dashed lines) and that derived from the SNO and Super-Kamiokande results (solid lines). The intercepts of these bands with the axes represent the  $\pm 1\sigma$  errors.

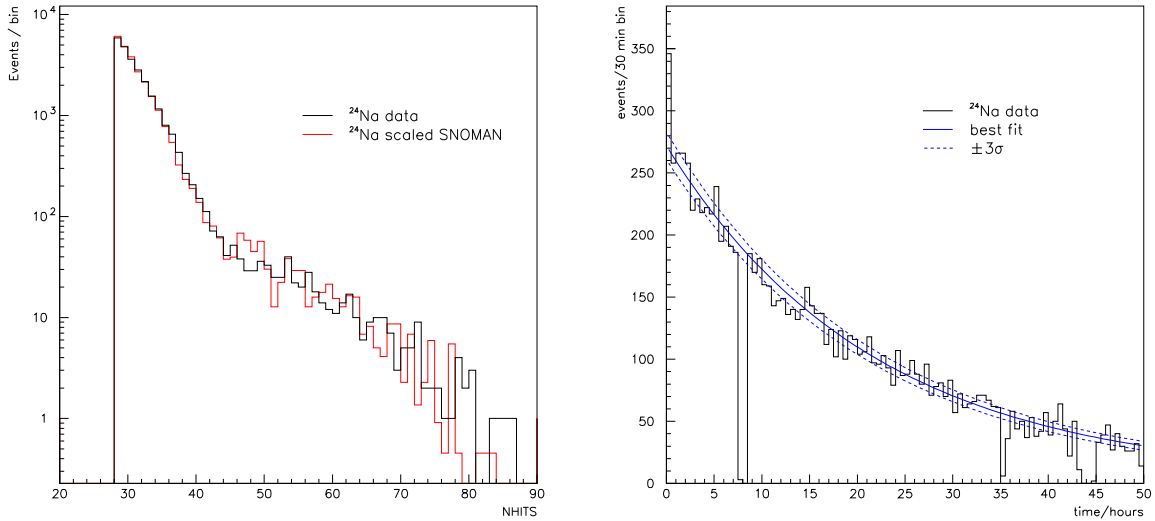


Figure 4: Left: Comparison of the data and Monte Carlo NHITS distributions. The sharply falling component at lower NHITS is from  $^{24}\text{Na}$  decays, and the higher NHIT bump is from neutron capture on  $^{35}\text{Cl}$ . Right: The decay of the activated  $^{24}\text{Na}$  in the  $\text{D}_2\text{O}$ .

The preferred value of the total active neutrino  $^8\text{B}$  flux is:

$$\Phi_{\text{SNO+SK}}^{\text{TOT}} = 5.44 \pm 0.99 \times 10^6 \text{ cm}^{-2} \text{ s}^{-1}$$

which is in good agreement with the standard solar model prediction:

$$\Phi_{\text{BEP01}}^{\text{TOT}} = 5.05_{-0.81}^{+1.01} \times 10^6 \text{ cm}^{-2} \text{ s}^{-1}$$

This is the first determination of the total active flux of  $^8\text{B}$  neutrinos generated by the Sun.

## 4 The NaCl Phase of the SNO Experiment

The deployment of NaCl to enhance the NC capability of the SNO detector began on May 28, 2001. The presence of NaCl in the  $\text{D}_2\text{O}$  causes the free neutron, produced by the NC interaction, to be captured by  $^{35}\text{Cl}$ . This produces an excited state of  $^{36}\text{Cl}$  which decays to its ground state via a cascade of  $\gamma$ -rays with a total energy of  $\sim 8.6$  MeV. The neutron detection efficiency is significantly enhanced, and the high multiplicity of the  $\gamma$ -ray cascade allows statistical separation from CC events based on the PMT hit pattern.

### 4.1 The $^{24}\text{Na}$ Calibration Source

The addition of NaCl to the  $\text{D}_2\text{O}$  presented the opportunity to deploy  $^{24}\text{Na}$  as a containerless source. This is desirable for two reasons:  $^{24}\text{Na}$   $\beta\gamma$  decays are similar to the  $\beta\gamma$  decays of  $^{208}\text{Tl}$  and  $^{214}\text{Bi}$ ; and a containerless source avoids the difficulties in modeling complex sources.

Activating  $^{23}\text{Na}$  in the  $\text{D}_2\text{O}$  was achieved by using the ‘super-hot’ thorium source, which produces  $2.0 \times 10^7 \pm 5\%$  2.614 MeV  $\gamma$ -rays per minute (producing neutrons from deuteron photodisintegration). Figure 4 shows the results of such a deployment. Comparing the detector response from the  $^{24}\text{Na}$  calibration source to Monte Carlo predictions gives confidence in, and allows systematic uncertainties to be assigned to, techniques designed to monitor the  $^{208}\text{Tl}$  and  $^{214}\text{Bi}$  levels within the  $\text{D}_2\text{O}$ .

## 5 Summary and Outlook

Two significant results are reported in this paper. The data from SNO represents the first direct evidence that there is an active non-electron flavour neutrino component in the solar neutrino flux. This is also the first experimental determination of the total flux of active  $^8\text{B}$  neutrinos, which is in good agreement with the solar model predictions.

The SNO Collaboration is now analysing the data from the pure  $\text{D}_2\text{O}$  phase with a lowered energy threshold. Efforts are devoted to understanding the low energy  $\beta\gamma$  decays of  $^{208}\text{Tl}$  and  $^{214}\text{Bi}$  and the photodisintegration contribution they make to the NC measurement.

## Acknowledgments

This research was supported by the Natural Sciences and Engineering Research Council of Canada, Industry Canada, National Research Council of Canada, Northern Ontario Heritage Fund Corporation and the Province of Ontario, the United States Department of Energy, and in the United Kingdom by the Science and Engineering Research Council and the Particle Physics and Astronomy Research Council. Further support was provided by INCO, Ltd., Atomic Energy of Canada Limited (AECL), Agra-Monenco, Canatom, Canadian Microelectronics Corporation, AT&T Microelectronics, Northern Telecom and British Nuclear Fuels, Ltd. The heavy water was loaned by AECL with the cooperation of Ontario Power Generation.

## References

1. B.T. Cleveland *et al.*, *Astrophys. J.* **496**, 505 (1998).
2. J.N. Abdurashitov *et al.*, *Phys. Rev. C* **60**, 055801 (1999).
3. W. Hampel *et al.*, *Phys. Lett. B* **447**, 127 (1999).
4. M. Altmann *et al.*, *Phys. Lett. B* **490**, 16 (2000).
5. K.S. Hirata *et al.*, *Phys. Rev. Lett.* **65**, 1297 (1990); K.S. Hirata *et al.*, *Phys. Rev. D* **44**, 2241 (1991), **45** 2170E (1992); Y. Fukuda *et al.*, *Phys. Rev. Lett.* **77**, 1683 (1996).
6. S. Fukuda *et al.*, *Phys. Rev. Lett.* **86**, 5651 (2001).
7. J.N. Bahcall, M. H. Pinsonneault, and S. Basu, astro-ph/0010346 v2.
8. A.S. Brun, S. Turck-Chièze, and J.P. Zahn, *Astrophys. J.* **525**, 1032 (1999); S. Turck-Chièze *et al.*, *Ap. J. Lett.*, v. **555** July 1, 2001.
9. The SNO Collaboration, *Nucl. Instr. and Meth.* **A449**, 172 (2000).
10. The SNO Collaboration, *Phys. Rev. Lett.* **87**, 071301 (2001).
11. S. Nakamura, T. Sato, V. Gudkov, and K. Kubodera, *Phys. Rev. C* **63**, 034617 (2001); M. Butler, J.-W. Chen, and X. Kong, *Phys. Rev. C* **63**, 035501 (2001); G. 't Hooft, *Phys. Lett.* **37B** 195 (1971).
12. M.R. Dragowsky *et al.*, *Nucl. Instr. and Meth.* **A481**, 284 (2002).
13. G.A. McGregor, *The Measurement of the Neutral Current Interaction at the Sudbury Neutrino Observatory*, D.Phil. thesis, University of Oxford (2002).